

## Optically Driven Rabi Oscillations and Adiabatic Passage of Single Electron Spins in Diamond

D. Andrew Golter and Hailin Wang

*Department of Physics and Oregon Center for Optics, University of Oregon, Eugene, Oregon 97403, USA*  
(Received 27 September 2013; revised manuscript received 6 January 2014; published 18 March 2014)

Rabi oscillations and adiabatic passage of single electron spins in a diamond nitrogen vacancy center are demonstrated with two Raman-resonant optical pulses that are detuned from the respective dipole optical transitions. We show that the optical spin control is nuclear-spin selective and can be robust against rapid decoherence, including radiative decay and spectral diffusion, of the underlying optical transitions. A direct comparison between the Rabi oscillation and the adiabatic passage, along with a detailed theoretical analysis, provides significant physical insights into the connections and differences between these coherent spin processes and also elucidates the role of spectral diffusion in these processes. The optically driven coherent spin processes enable the use of nitrogen vacancy excited states to mediate coherent spin-phonon coupling, opening the door to combining optical control of both spin and mechanical degrees of freedom.

DOI: [10.1103/PhysRevLett.112.116403](https://doi.org/10.1103/PhysRevLett.112.116403)

PACS numbers: 71.55.-i, 42.50.Ex, 42.50.Md, 78.47.jb

Negatively charged nitrogen vacancy (NV) centers in diamond feature long decoherence times for electron and nuclear spins, along with high-fidelity state preparation and optical readout [1–6]. The exquisite quantum control of electron and nuclear spin dynamics in a NV center has also led to the realization of quantum state transfer between electron and proximal nuclear spins [7,8]. A primary challenge for the use of NV centers in quantum information processing is to mediate and control entanglement between individual spin qubits. Spin entanglement of NV centers mediated by short-range dipole coupling or through spin-photon entanglement has been explored with remarkable successes [9–13]. It is not clear, however, that these approaches will be scalable.

Recent advances in quantum optomechanics have also stimulated strong interest in coupling electron spins to high- $Q$  nanomechanical oscillators and especially in using the mechanical degrees of freedom to mediate spin entanglement as well as spin-photon quantum interfaces [14–19]. Nearly all experimental efforts on coherent spin-phonon coupling with NV centers have thus far focused on the use of the ground-state spin-phonon coupling. Direct coupling between electron spins and a nanomechanical oscillator has been demonstrated recently via a mechanically driven spin transition [20]. Spin-phonon coupling in NV centers, however, can also be mediated through electron-phonon coupling of the NV excited states. The corresponding deformation potential is a few electron volts, several orders of magnitude greater than that of the ground-state spin-phonon coupling. For a  $\Lambda$ -type three-level system with two spin states as the lower states, phonon-assisted optical transitions can lead to phonon-assisted spin transitions. The effective Hamiltonian for this optically driven spin-phonon interaction is the same as that for the trapped ions [17]. Similar to trapped ions [21], entanglement of NV electron

spins can be generated via optical control of both the mechanical and spin degrees of freedom.

A crucial and fundamental issue for the pursuit of this solid-state analog of trapped ions is the need to control electron spin states through optical transitions, while avoiding the rapid decoherence of these transitions. In addition to radiative decay, optical transitions in solids are also subject to other environmental fluctuations such as spectral diffusion of the transition frequencies [22–24]. To take advantage of nuclear spins, it is also important that the optically driven spin dynamics be nuclear-spin selective.

Optical spin control can take place via either optically driven Rabi oscillations (ODROs) or stimulated Raman adiabatic passage (STIRAP). In this Letter, we report experimental demonstration of both ODROs and STIRAP of single electron spins in a NV center by using two Raman-resonant optical pulses that are detuned from the respective dipole optical transitions. A direct comparison between ODROs and STIRAP in a specially designed experiment, along with a detailed theoretical analysis based on the optical Bloch equations (OBE), provides significant insights into the connections and differences between them and also elucidates the role of spectral diffusion in these coherent spin processes. We show that optical spin control can be achieved, with negligible effects from decoherence of the underlying optical transitions. With a modest dipole detuning, the optical spin control becomes robust against radiative decay of the excited states. Although the ODROs are susceptible to spectral diffusion, the STIRAP is immune to the spectral diffusion as long as the adiabatic condition is satisfied. In addition, we also show that the optical spin control processes depend on the orientation of the adjacent  $^{14}\text{N}$  nuclear spin and are thus nuclear-spin selective.

The electronic ground states of NV centers are a spin triplet, characterized by  $m_s = 0$  and  $m_s = \pm 1$  states [25].

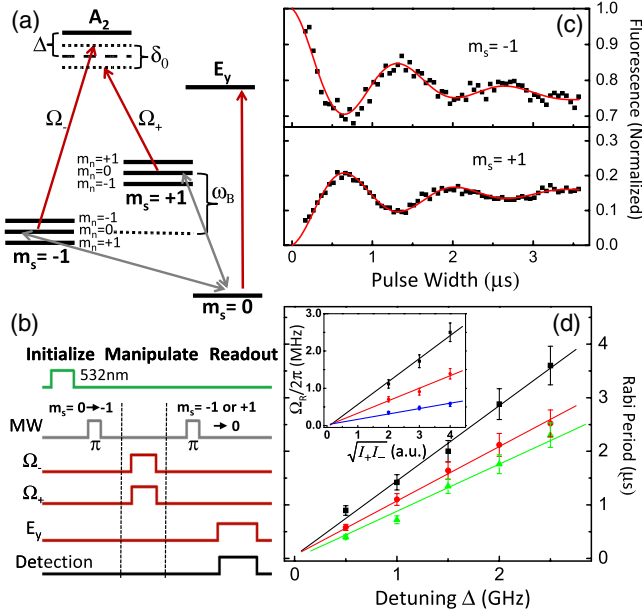


FIG. 1 (color online). (a) Energy level structure of a NV center, including the hyperfine splitting, Zeeman splitting ( $\omega_B$ ), and the relevant excited states. The arrows indicate the directions of the intended optical or MW excitations. (b) Pulse sequence used for ODROs. (c) ODROs of an electron spin. The fluorescence measures the population in the  $m_s = \pm 1$  states. The solid line is a numerical fit to a damped oscillation with an added slope due to optical pumping. (d) Period of the ODROs as a function of detuning for three different optical intensities. Inset: effective Rabi frequency as a function of the intensity for three different detunings.

Spin conserving optical transitions can take place between the ground states and the six excited states [26–28]. Figure 1(a) shows a  $\Lambda$ -type three-level system, with the two lower levels  $m_s = \pm 1$  coupling to excited state  $A_2$  via  $\sigma-$  and  $\sigma+$  polarized light, respectively. The three energy levels form a nearly closed system, with a small probability for an electron in state  $A_2$  to decay nonradiatively into the  $m_s = 0$  state [9]. For the  $m_s = \pm 1$  states, each electron spin state splits into three hyperfine states with a hyperfine splitting of 2.2 MHz [25], corresponding to nuclear spin projection with  $m_n = -1, 0, +1$  [see Fig. 1(a)].

In the limit that two simultaneous, Raman-resonant optical fields coupling to the two dipole transitions in the  $\Lambda$ -system are sufficiently detuned from the respective dipole transitions, the excited state dynamics can adiabatically follow the incident optical fields as well as the dynamics of the two spin states. In this limit, the  $\Lambda$ -type system in Fig. 1(a) can in principle be reduced to a two-level spin system, with the effective Rabi frequency for the optically driven spin transition given by [29]

$$\Omega_R = \Omega_+ \Omega_- / (2|\Delta|), \quad (1)$$

where  $\Omega_+$  and  $\Omega_-$  are the Rabi frequencies for the respective dipole optical transitions and  $\Delta$  is the average detuning of the optical fields from the respective dipole transitions. Optically driven spin transitions can also take place via

coherent population trapping (CPT) or a dark state [30]. In the limit that the  $\Lambda$ -type three-level system is in a dark state,

$$|\psi_d\rangle = [\Omega_-(t)|+1\rangle - \Omega_+(t)|-1\rangle] / \sqrt{\Omega_+^2(t) + \Omega_-^2(t)}, \quad (2)$$

the spin system can be controlled adiabatically by varying the relative amplitude of the optical fields through STIRAP (see the Supplemental Material [31]). CPT has been realized in NV centers [32–35]. All optical control of electron spins via a dark state has also been explored recently by tuning a NV center to an excited-state spin anticrossing [36].

Our experimental studies were carried out in a type IIa diamond at  $T \approx 5$  K in a close-cycled optical cryostat. A small magnetic field was applied to induce a Zeeman splitting,  $\omega_B = 150$  MHz, between the  $m_s = \pm 1$  states. A green 532 nm laser provided off-resonant NV excitation. A tunable ring laser at 637 nm was used for the two nearly resonant optical fields. Optical pulses of and relative detuning between these two fields were generated with acousto-optic modulators. Detailed information of the NV center used has been presented in an earlier study on CPT of electron spins [35].

As illustrated in Fig. 1(b), the single NV center was first initialized with a green laser pulse into the  $m_s = 0$  state. A microwave (MW)  $\pi$  pulse then prepared the NV in the  $m_s = -1$  state, with random nuclear spin orientation unless otherwise specified. In the manipulation step, two simultaneous square-shaped optical pulses were Raman resonant with the  $m_s = \pm 1$  states and were detuned from the  $A_2$  transition. The two optical fields had nearly equal peak intensity and were oppositely circularly polarized with an extinction ratio near 10:1. For the spin detection, the spin population in either the  $m_s = +1$  or  $m_s = -1$  state was measured with a two-step photoluminescence excitation (PLE)-based process. First, a MW  $\pi$  pulse drove the relevant spin population into the  $m_s = 0$  state. Second, the transition between the  $m_s = 0$  and  $E_y$  states was resonantly excited with a tunable diode laser, with the resulting fluorescence measured at the lower energy phonon sideband.

Figure 1(c) shows that the electron spin population oscillates with the duration of the incident optical pulses, where  $\Delta$  is set to  $-1.5$  GHz (blue detuned) and the optical pulses are Raman resonant with the spin states with  $m_n = 0$  (i.e.,  $\delta_0 = 0$  with  $\delta_n$  being the detuning from the respective Raman resonance for given  $m_n$ ). As expected from Eq. (1), the period of the oscillation determined from the experiments is proportional to  $|\Delta|$ ; the effective Rabi frequency  $\Omega_R$  is proportional to  $\sqrt{I_+ I_-}$  [see Fig. 1(d)], where  $I_+$  and  $I_-$  are the peak intensities for the respective optical pulses. As shown in Fig. 1(c), the ODROs feature a decay time of  $1.3 \mu\text{s}$ , compared with an excited state lifetime of 11.5 ns and an absorption linewidth of 500 MHz for single NVs [22–24]. The decay mechanisms of the ODROs will be discussed in detail later.

The ODROs shown in Fig. 1(c) depend on the orientation of the  $^{14}\text{N}$  nuclear spin associated with the NV center. For clarity, we have included in Fig. 2(a) the spectral response obtained in an earlier CPT experiment performed on the same NV center, where the three dips correspond to the Raman resonant condition associated with  $m_n = -1, 0, +1$ , respectively [35]. As shown in Fig. 2, ODROs of the electron spin are observed when the frequency difference between the two incident optical fields is at the dips of the CPT spectral response, i.e., when the  $m_n$ -dependent Raman resonant condition is satisfied. The oscillations, however, vanish when the frequency difference is midway between two dips [see Fig. 2(b)]. As long as  $\Omega_R$  is small compared with the relevant hyperfine splitting, the optically driven spin transitions are nuclear-spin selective.

For Figs. 1 and 2, the nuclear spin orientation is random and the ODROs are nuclear-spin selective. Thus, only 1/3 of the total electron population is involved in the ODROs. For ODROs with perfect fidelity, the minimum normalized fluorescence for the  $m_s = -1$  state is 2/3 and the maximum normalized fluorescence for the  $m_s = +1$  state is 1/3. Note that the decay of the electron population in the  $m_s = -1$  state shown in Fig. 2(b) provides a separate measure of the excitation of the  $A_2$  state and the subsequent optical pumping, i.e., decay of the electron from the  $A_2$  state to the  $m_s = +1$  as well as the  $m_s = 0$  state. The slow decay shown in Fig. 2(b) indicates that the optical pumping has a relatively minor contribution to the decay of the ODROs.

We have used the optical spin rotation to determine the dephasing time of the electron spin. For these experiments, the electron population was initialized into the  $m_s = -1$  state with a given nuclear spin orientation  $m_n$  using a nuclear-spin-selective MW  $\pi$  pulse. Two Raman-resonant optical pulse pairs then induced  $\pi/2$  rotations separated by time  $\tau$  [see

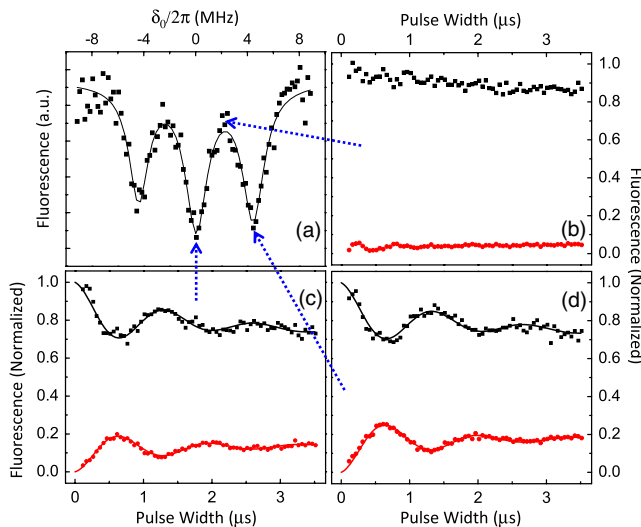


FIG. 2 (color online). Nuclear-spin-selective ODROs, with the detunings indicated in (a), the CPT spectral response. (b)–(d) The populations in the  $m_s = -1$  (top traces) and  $m_s = +1$  (bottom traces) states. Solid lines in (c) and (d) are numerical fits to damped oscillations.

Fig. 3(a)]. After the second  $\pi/2$  rotation, the population in the  $m_s = +1$  state was measured as before. Figures 3(b)–3(d) show the electron spin precessions obtained with  $m_n = 0, -1, +1$ , respectively, with  $\delta_0 = 1.4$  MHz. The solid lines in these figures show a numerical fit to  $\exp[-(\tau/T_2^*)^2] \cos(2\pi\delta_n)$  with  $T_2^* = 1 \mu\text{s}$  [7], in agreement with separate Ramsey fringe experiments performed using MW-driven  $\pi/2$  pulses. In Fig. 3(e), the electron population was initialized into the  $m_s = -1$  state with a random nuclear spin orientation. The solid line in Fig. 3(e) shows the sum of the three numerical fits obtained for individual  $m_n$ , with no adjustable parameters except for an overall scaling factor. These experiments show that the optically driven spin rotation is as effective as the conventional MW-driven spin rotation.

Optically driven coherent spin evolution can take place via STIRAP as well as the ODROs. For a detailed understanding of the optically driven coherent spin dynamics, we have devised a method to perform and compare both the ODROs and STIRAP in a single experiment. The pulse sequence used is similar to that in Fig. 1, but now we tailor the temporal line shape of the Raman-resonant optical pulses and delay the two pulses relative to each other. As shown in Fig. 4(a), the rising edge of the  $\Omega_-$  pulse and the trailing edge of the  $\Omega_+$  pulse are characterized by time  $t_{\text{rise}}$ . The separation between the rising edge of the  $\Omega_+$  pulse and the trailing edge of the  $\Omega_-$  pulse is defined as  $T$ . With the  $\Omega_+$  laser on and the  $\Omega_-$  laser off and with the electron initially in state  $m_s = -1$ , the system is automatically in the

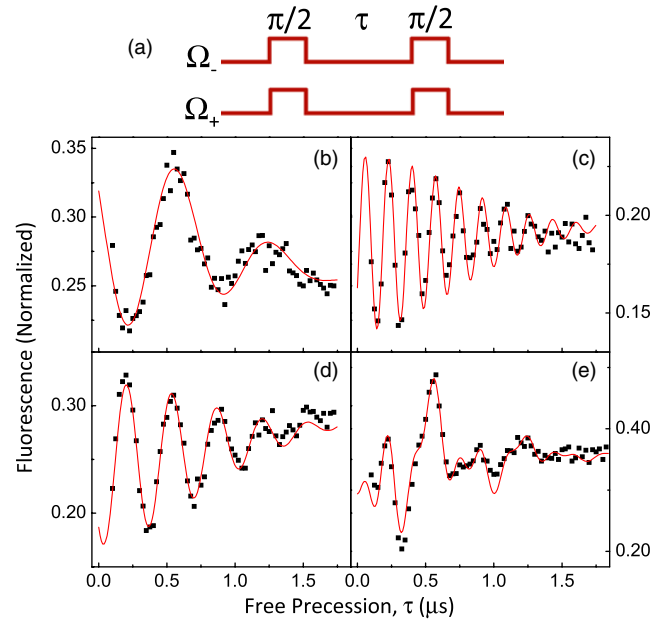


FIG. 3 (color online). (a) Pulse sequence used for the Ramsey fringe experiment. (b)–(e) Free induction decays of an electron spin with  $\Omega_R/2\pi = 2.5$  MHz and  $\Delta = -1$  GHz. For (b), (c), and (d), nuclear-spin-selective MW  $\pi$  pulses were used to prepare the electron in the  $m_s = -1$  and  $m_n = 0, -1$ , and  $+1$  hyperfine states, respectively. For (e), the electron was prepared in the  $m_s = -1$  state with random nuclear spin orientation. Solid lines are numerical fits as discussed in the text.

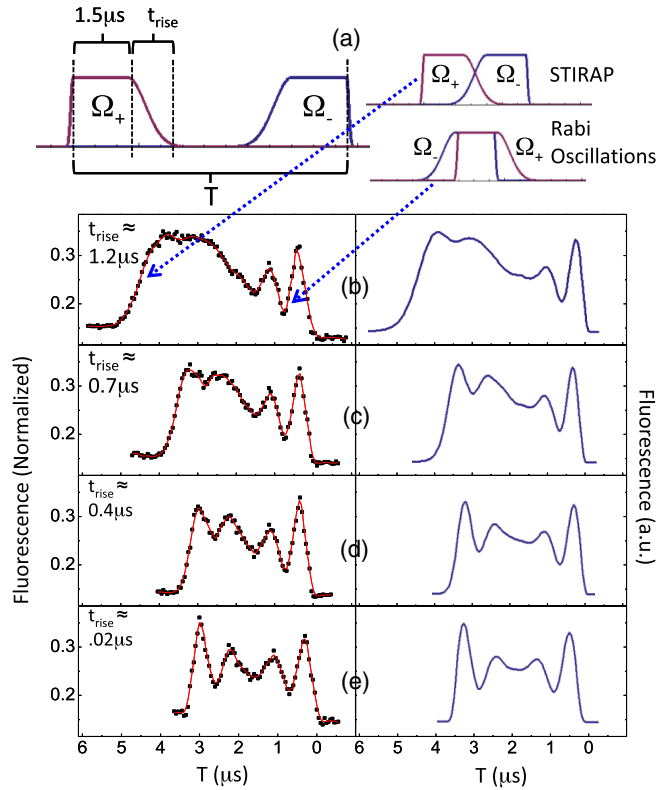


FIG. 4 (color online). (a) The temporal line shapes of the two optical pulses used for the experiment, for which the population in state  $m_s = +1$  was measured as a function of delay  $T$  between the two pulses. (b)–(e) Left column: experimental results obtained with different  $t_{\text{rise}}$ , as indicated in the figure. Solid lines are guides to the eye. Right column: theoretical calculations using parameters of the experiments in the left column.

dark state without any additional preparation. As  $\Omega_+$  ramps down and  $\Omega_-$  ramps up [Fig. 4(a)], the electron can be transferred to state  $m_s = +1$  via STIRAP [see Eq. (2)], for which the adiabatic condition requires that the time scale of transfer is slow compared with the relevant Rabi period.

Figure 4 reveals the close connections as well as the differences between the ODROs and STIRAP. For Figs. 4(b)–4(e) (left column), the population in the  $m_s = +1$  state, following the application of the two optical

pulses, was measured as a function of  $T$ , with  $\Delta = -0.9$  GHz and with other conditions remaining the same as those in Fig. 1. For  $t_{\text{rise}} = 1.2 \mu\text{s}$ , STIRAP occurs as the trailing edge of the  $\Omega_+$  pulse overlaps with the rising edge of the  $\Omega_-$  pulse [see Fig. 4(b)]. ODROs take place when the peak amplitudes of the two optical pulses overlap in time. For decreasing  $t_{\text{rise}}$  [see Figs. 4(c)–4(d)], the adiabatic condition breaks down and the STIRAP transitions into the ODROs, confirming that adiabatic transfer via the dark state can only take place on a time scale slower than the Rabi period.

For a detailed theoretical description of the experiments, we have modeled the spin dynamics with the OBE for a  $\Lambda$ -type three-level system (see the Supplemental Material [31] and Ref. [37]). The right column of Figs. 4(b)–4(e) plots the calculation under the conditions of the experiments in the left column, where we have used  $T_2 = 200 \mu\text{s}$  for the electron spin and an intrinsic decoherence rate  $\gamma/2\pi = 7$  MHz for the  $A_2$  transitions, with all other parameters derived from the experiments. Spectral diffusion of the optical transition was modeled as an inhomogeneous broadening, with a linewidth of 500 MHz as determined from PLE spectra [22,24]. Figure 4 shows an overall good agreement between the theory and experiment (see the Supplemental Material [31]).

The calculations in Fig. 5 single out the effects of individual decoherence mechanisms on the ODROs and STIRAP shown in Fig. 4(b), further highlighting the differences between these two coherent spin processes. As shown in Fig. 5(a), effects of radiative decay become negligible with a modest dipole detuning  $\Delta$ . For spectral diffusion, the fluctuations in  $\Delta$  induce corresponding changes in the effective Rabi frequency  $\Omega_R$  [see Eq. (1)], resulting in strong damping of the ODROs as shown in Fig. 5(b). In contrast, the STIRAP is independent of  $\Omega_R$ , as long as the adiabatic condition is maintained, and is thus highly robust against the spectral diffusion. Spin dephasing due to the nuclear spin bath affects the STIRAP and ODROs nearly equally, as shown in Fig. 5(c). Overall, ODROs are limited by both spectral diffusion and spin dephasing. Optical spin control via STIRAP, however, is primarily limited by spin dephasing. In this regard, while ODROs are

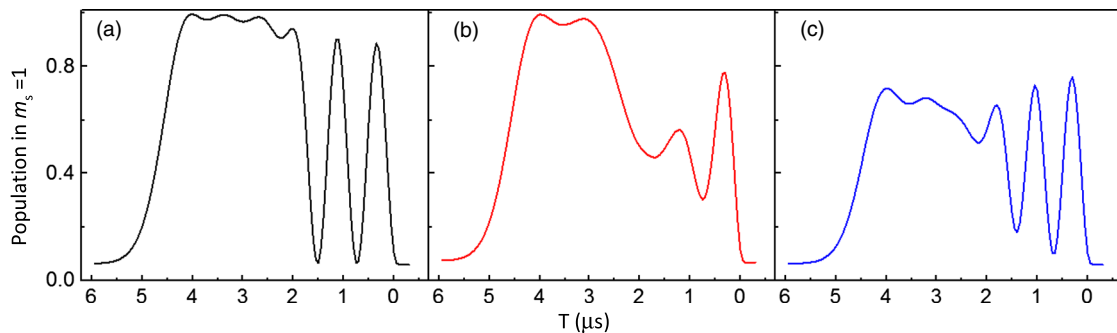


FIG. 5 (color online). Calculation of STIRAP and ODROs in Fig. 4(b), including spin and radiative decoherences and selective other decoherence mechanisms. (a) No spin dephasing and no spectral diffusion. (b) No spin dephasing, but including spectral diffusion. (c) No spectral diffusion, but including spin dephasing.

preferred for fast spin control, STIRAP is more robust when effects of spectral diffusion become significant. Note that spin dephasing can be overcome with dynamical decoupling or with isotopically pure diamond [1,38].

In summary, we have demonstrated ODRs and STIRAP of single electron spins in diamond. With a modest dipole detuning, optical spin control can be realized, with negligible effects from decoherence processes, including rapid radiative decay and large spectral diffusion, of the underlying optical transitions. These remarkable coherent spin phenomena should enable the use of NV excited states to mediate coherent spin-phonon coupling and, in particular, the use of an optically driven spin-phonon system to realize a solid-state analog of trapped ions. Our experimental approaches can also be extended to other emerging spin systems such as SiC [39].

This work is supported by NSF under Grant No. 1005499.

- 
- [1] G. Balasubramanian, P. Neumann, D. Twitchen, M. Markham, R. Kolesov, N. Mizuochi, J. Isoya, J. Achard, J. Beck, J. Tissler, V. Jacques, P.R. Hemmer, F. Jelezko, and J. Wrachtrup, *Nat. Mater.* **8**, 383 (2009).
- [2] P.C. Maurer, G. Kucsko, C. Latta, L. Jiang, N. Y. Yao, S. D. Bennett, F. Pastawski, D. Hunger, N. Chisholm, M. Markham, D. J. Twitchen, J. I. Cirac, and M. D. Lukin, *Science* **336**, 1283 (2012).
- [3] T. van der Sar, Z. H. Wang, M. S. Blok, H. Bernien, T. H. Taminiau, D. M. Toyli, D. A. Lidar, D. D. Awschalom, R. Hanson, and V. V. Dobrovitski, *Nature (London)* **484**, 82 (2012).
- [4] L. Robledo, L. Childress, H. Bernien, B. Hensen, P. F. A. Alkemade, and R. Hanson, *Nature (London)* **477**, 574 (2011).
- [5] L. Jiang, J. S. Hodges, J. R. Maze, P. Maurer, J. M. Taylor, D. G. Cory, P. R. Hemmer, R. L. Walsworth, A. Yacoby, A. S. Zibrov, and M. D. Lukin, *Science* **326**, 267 (2009).
- [6] P. Neumann, J. Beck, M. Steiner, F. Rempp, H. Fedder, P. R. Hemmer, J. Wrachtrup, and F. Jelezko, *Science* **329**, 542 (2010).
- [7] L. Childress, M. V. G. Dutt, J. M. Taylor, A. S. Zibrov, F. Jelezko, J. Wrachtrup, P. R. Hemmer, and M. D. Lukin, *Science* **314**, 281 (2006).
- [8] M. V. G. Dutt, L. Childress, L. Jiang, E. Togan, J. Maze, F. Jelezko, A. S. Zibrov, P. R. Hemmer, and M. D. Lukin, *Science* **316**, 1312 (2007).
- [9] E. Togan, Y. Chu, A. S. Trifonov, L. Jiang, J. Maze, L. Childress, M. V. G. Dutt, A. S. Sorensen, P. R. Hemmer, A. S. Zibrov, and M. D. Lukin, *Nature (London)* **466**, 730 (2010).
- [10] A. Sipahigil, M. L. Goldman, E. Togan, Y. Chu, M. Markham, D. J. Twitchen, A. S. Zibrov, A. Kubanek, and M. D. Lukin, *Phys. Rev. Lett.* **108**, 143601 (2012).
- [11] H. Bernien, B. Hensen, W. Pfaff, G. Koolstra, M. S. Blok, L. Robledo, T. H. Taminiau, M. Markham, D. J. Twitchen, L. Childress, and R. Hanson, *Nature (London)* **497**, 86 (2013).
- [12] P. Neumann, N. Mizuochi, F. Rempp, P. Hemmer, H. Watanabe, S. Yamasaki, V. Jacques, T. Gaebel, F. Jelezko, and J. Wrachtrup, *Science* **320**, 1326 (2008).
- [13] F. Dolde, I. Jakobi, B. Naydenov, N. Zhao, S. Pezzagna, C. Trautmann, J. Meijer, P. Neumann, F. Jelezko, and J. Wrachtrup, *Nat. Phys.* **9**, 139 (2013).
- [14] P. Rabl, P. Cappellaro, M. V. Gurudev Dutt, L. Jiang, J. R. Maze, and M. D. Lukin, *Phys. Rev. B* **79**, 041302 (2009).
- [15] K. Stannigel, P. Rabl, A. S. Sorensen, P. Zoller, and M. D. Lukin, *Phys. Rev. Lett.* **105**, 220501 (2010).
- [16] S. Kolkowitz, A. C. B. Jayich, Q. P. Unterreithmeier, S. D. Bennett, P. Rabl, J. G. E. Harris, and M. D. Lukin, *Science* **335**, 1603 (2012).
- [17] A. Albrecht, A. Retzker, F. Jelezko, and M. B. Plenio, *New J. Phys.* **15**, 083014 (2013).
- [18] S. D. Bennett, N. Y. Yao, J. Otterbach, P. Zoller, P. Rabl, and M. D. Lukin, *Phys. Rev. Lett.* **110**, 156402 (2013).
- [19] K. V. Keesidis, S. D. Bennett, S. Portolan, M. D. Lukin, and P. Rabl, *Phys. Rev. B* **88**, 064105 (2013).
- [20] E. R. MacQuarrie, T. A. Gosavi, N. R. Jungwirth, S. A. Bhawe, and G. D. Fuchs, *Phys. Rev. Lett.* **111**, 227602 (2013).
- [21] D. Leibfried, R. Blatt, C. Monroe, and D. Wineland, *Rev. Mod. Phys.* **75**, 281 (2003).
- [22] P. Tamarat, T. Gaebel, J. R. Rabeau, M. Khan, A. D. Greentree, H. Wilson, L. C. L. Hollenberg, S. Prawer, P. Hemmer, F. Jelezko, and J. Wrachtrup, *Phys. Rev. Lett.* **97**, 083002 (2006).
- [23] Y. Shen, T. M. Sweeney, and H. Wang, *Phys. Rev. B* **77**, 033201 (2008).
- [24] Kai-Mei C. Fu, C. Santori, P. E. Barclay, L. J. Rogers, N. B. Manson, and R. G. Beausoleil, *Phys. Rev. Lett.* **103**, 256404 (2009).
- [25] M. W. Doherty, F. Dolde, H. Fedder, F. Jelezko, J. Wrachtrup, N. B. Manson, and L. C. L. Hollenberg, *Phys. Rev. B* **85**, 205203 (2012).
- [26] J. R. Maze, A. Gali, E. Togan, Y. Chu, A. Trifonov, E. Kaxiras, and M. D. Lukin, *New J. Phys.* **13**, 025025 (2011).
- [27] A. Batalov, V. Jacques, F. Kaiser, P. Siyushev, P. Neumann, L. J. Rogers, R. L. McMurtrie, N. B. Manson, F. Jelezko, and J. Wrachtrup, *Phys. Rev. Lett.* **102**, 195506 (2009).
- [28] G. D. Fuchs, V. V. Dobrovitski, R. Hanson, A. Batra, C. D. Weis, T. Schenkel, and D. D. Awschalom, *Phys. Rev. Lett.* **101**, 117601 (2008).
- [29] T. M. Sweeney, C. Phelps, and H. L. Wang, *Phys. Rev. B* **84**, 075321 (2011).
- [30] K. Bergmann, H. Theuer, and B. W. Shore, *Rev. Mod. Phys.* **70**, 1003 (1998).
- [31] See Supplemental Material at <http://link.aps.org/supplemental/10.1103/PhysRevLett.112.116403> for a more detailed theoretical analysis of the experimental results as well as discussions on dark states and adiabatic state transfer.
- [32] E. Togan, Y. Chu, A. Imamoglu, and M. D. Lukin, *Nature (London)* **478**, 497 (2011).
- [33] C. Santori, P. Tamarat, P. Neumann, J. Wrachtrup, D. Fattal, R. G. Beausoleil, J. Rabeau, P. Olivero, A. D. Greentree, S. Prawer, F. Jelezko, and P. Hemmer, *Phys. Rev. Lett.* **97**, 247401 (2006).
- [34] P. R. Hemmer, A. V. Turukhin, M. S. Shahriar, and J. A. Musser, *Opt. Lett.* **26**, 361 (2001).
- [35] D. A. Golter, K. N. Dinyari, and H. L. Wang, *Phys. Rev. A* **87**, 035801 (2013).
- [36] C. G. Yale, B. B. Buckley, D. J. Christle, G. Burkard, F. J. Heremans, L. C. Bassett, and D. D. Awschalom, *Proc. Natl. Acad. Sci. U.S.A.* **110**, 7595 (2013).
- [37] M. O. Scully and M. S. Zubairy, *Quantum Optics* (Cambridge University Press, Cambridge, England, 1997).
- [38] G. de Lange, Z. H. Wang, D. Riste, V. V. Dobrovitski, and R. Hanson, *Science* **330**, 60 (2010).
- [39] W. F. Koehl, B. B. Buckley, F. J. Heremans, G. Calusine, and D. D. Awschalom, *Nature (London)* **479**, 84 (2011).